

Formation and stabilization of ZnO nanoparticles inside MCM-48 porous support via post-synthetic organometallic route

Mahuya Bandyopadhyay^{1*}, Hermann Gies², Wolfgang Grünert³, Maurits Van Den Berg⁴, Alexander Birkner⁵

¹Institute of Infrastructure, Technology, Research and Management, IITRAM, Maninagar, Ahmedabad, Gujarat, India

²Laboratory of Crystallography, Ruhr University Bochum, 44780 Bochum, Germany

³Laboratory of Industrial Chemistry, Ruhr University Bochum, 44780 Bochum, Germany

⁴Sachtleben Pigment GmbH, 47829, Krefeld, Germany

⁵Laboratory of Physical Chemistry I, Ruhr University Bochum, 44780 Bochum, Germany

*Corresponding author. Tel: (+91) 990-998-5869; E-mail: mahuyabandyopadhyay@iitram.ac.in

Received: 12 June 2015, Revised: 26 August 2015 and Accepted: 01 September 2015

ABSTRACT

The interpenetrating 3-dimensional channel system of silica MCM-48 has been selected for the deposition of ZnO nanoparticles. The post-synthetic organometallic route was employed to load the mesoporous silica with ZnO-precursor molecule. Calcination of the composite transformed the organometallic sorbate to the corresponding metal oxide. X-ray powder diffraction, N₂-Adsorption and TEM measurement have supported the efficient loading and growth of ZnO particles in the channels of mesoporous silica matrix. EXAFS analysis (ZnK-edges) also complemented the metal uptake. Presence of nano-dispersed and nanosized ZnO particles confined by the mesoporous pore system was established by TEM and EXAFS analysis. Copyright © 2015 VBRI Press.

Keywords: Mesoporous; nanoparticles; TEM; EXAFS.

Introduction

The nanocrystalline metal/metal oxides have attracted considerable attention in the development of advanced quantum-confined electronic and optoelectronic devices such as lasers, switches [1], catalyst [2], photocatalyst [3], and solar cells [4]. Properties of materials manipulated by the quantum-size effect of nanocrystals have also been explored for remediation and other environmental issues. As an example, ZnO nanocrystals have been explored and applied as potential photocatalyst for the degradation of organic pollutants in water and air because of their non-toxicity, lower cost and higher reactivity [3]. Also, functional nano-micro ZnO structures have found applications in biomedical and consumer products with minimization of toxicity [5].

In order to control the stability of the ZnO, colloidal solutions [6], porous glasses [7], polymers [8] and alumina matrices have been used as hosts for the metal oxide nanoparticles. In another field of applications, binary oxide, sulfide and selenide semiconductors (e.g., ZnO, Cu₂O, ZnS, CdS, PbS, CdSe, PbSe and many others) have attracted great attention because of their specific electronic and optical properties, which differ significantly from the

bulk materials. A simple flame transport approach was utilized by Mishra *et al.* to prepare macroscopically flexible and porous 3D semiconductor networks from interpenetrating nanostructures of different metals [9]. The work was further extended to study the prophylactic, therapeutic and neutralizing effects against viral infection [10]. Extensive work by Zeng *et al.* on optical and electronic applications of nanostructured ZnO concludes that, not only the composition but tuning the material properties is one of the important criteria for studying contemporary nanotechnology [11]. Tian *et al.* reported systematic synthesis of large arrays of oriented ZnO nanostructures by controlling heterogeneous nucleation and growth in aqueous solution at low temperature [12].

However, comparatively low chemical and temperature stability of nanoparticles usually results in distortion of originally adjusted parameters due to aggregation processes or chemical reactions with their surroundings, limiting practical application of purely nanocrystalline systems. To overcome the aggregation problem, encapsulation of the nanoparticles in a chemically inert and transparent matrix is considered to be one of the best options. The other important advantage of implementation of the matrix techniques is the possibility of accurately controlling

dispersion of nanoparticles. Obviously the degree of dispersion of the nanoparticles depends on the uniformity of the pores inside the matrix. To choose such matrices possessing uniform pore structure with accurately controlled diameter, is a great challenge. The most known and promising solid state nano-reactors having uniform pore structure at the nano level are crystalline porous materials (zeolites) and ordered mesoporous silica and porous alumina [13, 14]. It was recognized that the incorporation of nanosized materials in zeolitic pores has specific advantages; however, the pore size of these materials of less than 2 nm limits their applicability. Therefore the discovery of ordered mesoporous materials has broadened the scope of these applications.

Another area of application-oriented interest for OMMs (ordered mesoporous materials) is their use as carrier for functional molecules or nanoparticles [15-18]. Of particular interest are the silica based OMMs because of their transparency, high thermal and chemical stability, and their mechanical robustness. The advancement of ordered mesoporous materials has inspired areas of work like intra pore formation of metal aggregates for the catalytic conversion of bulky molecules. Encapsulation process favors high dispersion of particles. Through the OMM silica-framework, it also protects the functional molecules or nanoparticle from oxidation, decomposition or dissolution in the course of reaction with solvent or atmosphere [19, 20].

MCM-48, a so-far relatively unexploited mesoporous siliceous molecular sieve, has been investigated in the present work. This material has certain advantages over MCM-41, another related but structurally different mesoporous matrix. The cubic symmetry of MCM-48 with its three-dimensional framework periodicity and presence of two interpenetrating pore systems make it very special. Compared to one- or two dimensional pore systems, the three-dimensional pore of MCM-48 generates more resistance against pore blockage and provides a more efficient diffusion pathway. Studies on nanoparticles of Fe, Co, and Ni oxides in MCM-48 host system have been reported by Köhn *et al.* [21]. The chosen metals are of high interest due to their wide range of applications in catalysis.

Cu-Zn mixed oxides are of great importance for industrial-scale catalytic processes such as low pressure methanol formation from synthesis gas and steam reforming of methanol yielding H₂ and CO₂ [22]. We have already reported Cu-Zn mixed oxides [23], TiO₂ nanoparticles [24], and Au-TiO₂ nanoparticles [25] incorporated inside mesoporous MCM-48 matrix. We explored the use of TiO₂/MCM-48 as a matrix for the formation of thermally stable nano sized gold particles and the use of the composites as CO-oxidation catalyst. The composite was catalytically active even at -30 °C and encapsulation in mesoporous matrix prevents gold nano particle from sintering up to at least 200 °C without any loss in catalytic activity. The work reported here is part of an effort to prepare and explore encapsulated Cu/ZnO methanol synthesis catalysts in microporous and mesoporous matrices. Cu-Zn mixed oxides were incorporated in MCM-48 by post-synthetic wet-impregnation method. This wet impregnation process led to

the formation of nano-dispersed Cu-oxide in organized particles; however, Zn-oxide showed different behavior. Instead of formation of nanoparticles, it most likely spread on the surface of the silicate channel wall and partially reacted with the support. To overcome this problem, incorporation of ZnO via a different route was crucial.

In this report, formation of ZnO nanoparticles inside the poresystem of mesoporous silica-MCM-48 as support via organometallic route has been explored. The corresponding oxide is formed through thermal decomposition of the sorbate. The product was analyzed by powder XRD experiments followed by EXFAS, TEM and N₂-adsorption.

Experimental

Material synthesis

MCM-48 was synthesized according to literature procedures [23]. 1 molar NaOH was taken in a polypropylene bottle and, to it, CTACI (cetyltrimethylammonium-chloride, Aldrich, 25 % solution in water) was added drop-wise under continuous stirring. After 15 minutes of stirring, tetraethoxysilane, TEOS (Merck) was added drop-wise and the stirring was continued until the gel was homogeneous. The gel preparation was done in a water bath at 40-50 °C. The final molar gel composition of the synthesis mixture was 1 (TEOS): 0.70(CTACI): 0.5 (NaOH): 64 (H₂O). The sealed bottle containing the gel was transferred into an oven at 90 °C and the synthesis was continued for 4 days. Afterwards, the sample was washed thoroughly with distilled water and dried overnight at room temperature followed by washing again with a mixture of H₂O, ethanol and HCl (molar ratio 90:5:10), and drying at room temperature. For calcination the sample was heated at 540 °C for 5 h.

Zn modified MCM-48 was prepared by organometallic route. In this process, first MCM-48 was dried in a vacuum oven at 180 °C for 17 h. The sample was then transferred to a three-mouth flask. Finally Zn (C₂H₅)₂ was added into the flask followed by the addition of toluene as solvent. The mixture was stirred at room temperature for 6 h, filtered off and washed with toluene. The solid was dried overnight at room temperature before calcining at 540 °C in air for 5 h (heating ramp 1 °C/min). The ZnO-MCM-48 materials prepared via aqueous [23] and organometallic routes were marked by the labels (aq) and (om), respectively.

Characterizations

Powder X-ray powder diffraction experiments were carried out using a Siemens D5000 diffractometer with Cu-K α ₁ radiation in Debye-Scherrer geometry using capillary sample holders. The N₂ adsorption measurements were performed with a Quantachrome Autosorb automated gas sorption system using the Autosorb software. Transmission electron microscopy (TEM) was performed using a Hitachi H-8100 model operating at 200 kV.

X-ray absorption spectra (Zn K-edge at 9.659 eV) were measured at HasyLab E4 station (Hamburg) using a Si (111) double crystal monochromator detuned to 70 % maximum intensity to exclude higher harmonics present in the X-ray beam. The spectra $\mu(k)$ were measured in transmission

mode using ionization chambers, with the sample at liquid nitrogen temperature. Samples were pressed into self-supporting discs of suitable thickness and stored in ambient atmosphere.

Data treatment was carried out using the software package VIPER [26]. For background subtraction a Victoreen polynomial was fitted to the pre-edge region. A smooth atomic background, $\mu_0(k)$, was evaluated using smoothed cubic splines. The radial distribution function $FT[k^2](k)$ was obtained by fourier transformation of the k^2 -weighted experimental function $\chi(k) = (\mu(k) - \mu_0(k)) / \mu_0(k)$ multiplied by a Bessel window. For the determination of structural parameters, theoretical references calculated by the FEFF8.10 code were used [27]. To minimize the number of free parameters, equal backscatters were fitted with the same Eo-shift wherever possible (variations of ± 1 eV admitted).

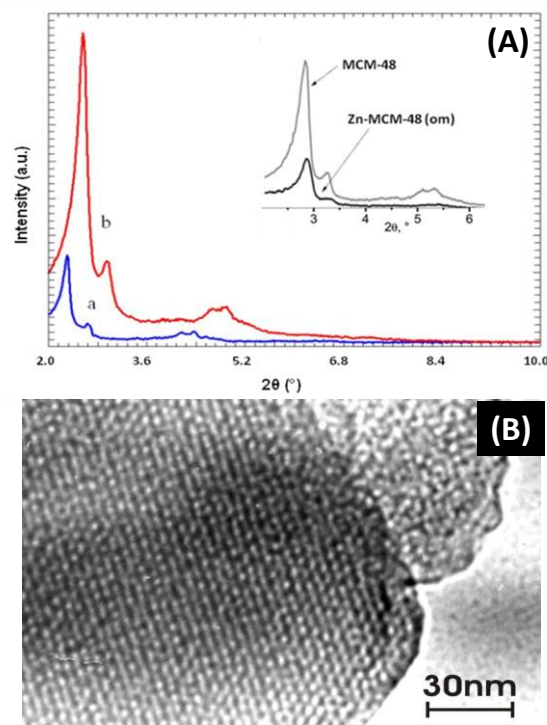


Fig. 1. (A) Powder XRD patterns of siliceous MCM-48 samples: (a) as-made (b) calcined. Inset: Siliceous calcined MCM-48 and Zn-loaded MCM-48 by organometallic route and (B) TEM image of an isolated MCM-48 particle loaded with ZnO (Organometallic route).

Results and discussion

Typical powder XRD patterns (**Fig. 1(A)**) of MCM-48 materials reveal excellent crystallinity of the samples synthesized from conventional hydrothermal synthesis procedures. The diagram showed a $\sim 30\%$ decrease in unit cell volume caused by the condensation of silanol groups after calcination. This phenomenon is supported by shift of the $d(211)$ from 38.41\AA to 34.24\AA , and (211) -peak from $\sim 2.30^\circ$ to $\sim 2.56^\circ$ 2θ , respectively. Calcination led to increase in diffraction peak intensities because of intensified diffraction contrast between channel pore and wall after the removal of the surfactant template [28].

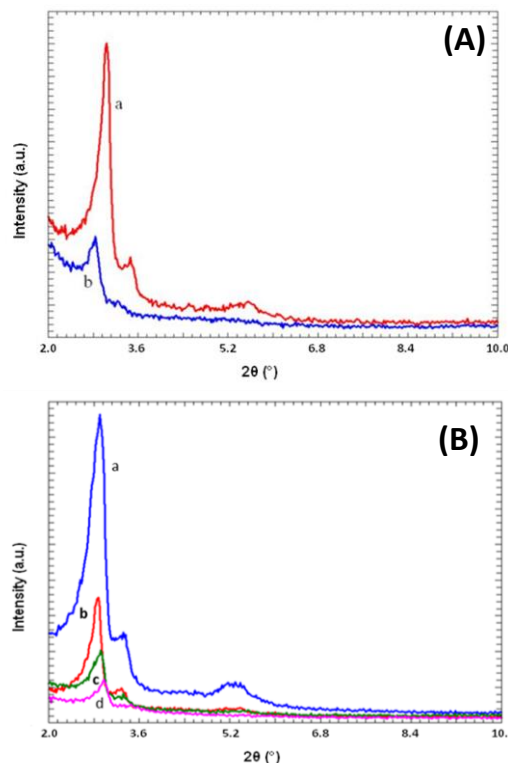


Fig 2. (A) Powder XRD patterns of calcined MCM-48 samples after ZnO loading: (a) Zn-acetate was used as Zn source (aqueous) and (b) diethylzinc was used as Zn source (organometallic). and (B) XRD patterns of successive loading of MCM-48 by zinc acetate: (a) calcined MCM-48 (b) 1st loaded (c) 2nd loaded (d) 3rd loaded.

The calcined and dried MCM-48 was treated with a solution of $(C_2H_5)_2Zn$ and recovered by filtration. The scattering contrast between pore and pore wall in MCM-48 decreases considerably after the impregnation of MCM-48 with the metal salt solution (**Fig. 1(inset)**). The introduction of the metal-organic molecule led to a strong reduction of a low angle XRD peaks indicative of the meso-character of the porous matrix. This effect can be caused by either lattice destruction or successful introduction of heavy elements into the pore system which decrease scattering contrast [23]. The higher the electron density of a sorbate molecule the lower the scattering contrast and, therefore, the lower the peak intensity in the powder diagram is. However, powder XRD cannot rule out degradation of the mesoporous framework. But from the TEM image in **Fig. 1(B)**, it is clear that the mesoporous particles are well aligned with respect to the electron beam, thereby the periodicity of the silica framework is maintained. After impregnation and calcination of the material, TEM image proves that the structure of the mesoporous silica framework is stable and highly crystalline without any damage of the framework. In order to check for bulk oxide signals, powder XRD-diagrams of the composite have been recorded up to 2° value of 50° . No additional diffraction peak was observed even after extended exposure experiments. This is in agreement with the expected line broadening of particles of less than 50\AA diameter with high disorder. This systematic change in scattering properties of mesoporous materials is one of the indications of metal salt uptake inside the channel pores and its thermal decomposition to the corresponding oxide.

However, in cases where the segregation and precipitation of metal oxide particles on the outer surface was observed in the TEM, bulk signals showed up in the XRD-diagram. Instead, the presence of XRD-signals of bulk oxides as indicator of externally precipitated sorbate was considered.

The XRD pattern of two different ZnO-MCM-48 samples prepared from organometallic and aqueous route is depicted in **Fig. 2(A)** and stepwise impregnation of MCM-48 by Zn-acetate in **Fig. 2(B)**.

In the aqueous route the peak intensity decay of the reflections was much more prominent than after organometallic zinc introduction; however, the reflection height of Zn-MCM-48 (om) fell more than that of the Zn-MCM-48 (aq), supporting high metal uptake via organometallic route. In fact, the metal uptake was found by ICP to be much higher in organometallic route (17 wt %) than the aqueous route (7 wt % after 3rd impregnation).

Using a calcined, empty MCM-48 sample as reference N_2 sorption measurements show that the pore diameter as well as surface area decreases after impregnation. The porosity results are shown in **Table 1**.

Table 1. Surface characteristics or porosity data for ordered MCM-48 solids, before and after ZnO impregnation: (a) ZnO loaded by aqueous route and (b) by organometallic route.

Sample	BET Surface area (m ² /g)	Pore diameter (Å)	Pore volume (cm ³ /g)
MCM-48, calcined	1257	25	1.8
(a) ZnO-MCM-48, 3rd impg.	860	20	0.61
(b) ZnO-MCM-48	700	20	0.63

The isotherms of MCM-48 are associated, as known from the literature, with a sharp increase around p/p_0 0.3, which indicates a narrow pore size distribution. The MCM-48 sample that has been used for an impregnation has a lower pore volume and at the same time, a smaller average pore diameter (**Fig. 3**).

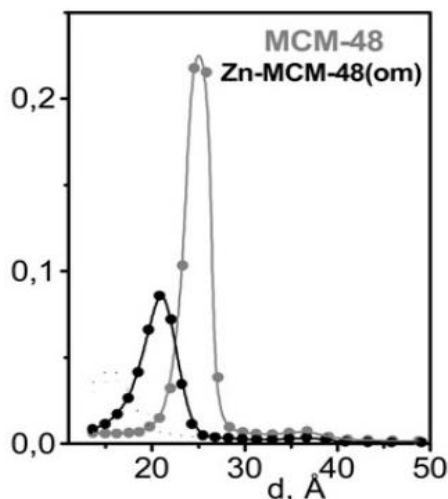


Fig. 3. Pore size distribution curve of MCM-48 compared with Zn-loaded MCM-48 (organometallic).

The introduction of Zn in the mesopore system leads to a substantial changes in the porosity measurements. After metal loading the material still has high surface area that means pores are still accessible. Use of diethyl zinc

decreases the pore volume and at the same time the isotherm at p/p_0 0.3 becomes less steep, indicating broader pore size distribution, which is shifted towards lower average pore diameter with decrease of 56 % of surface area (1257 to 700 m²/g) from a pure MCM-48 material. This decrease of surface area from 1257 to 700 m²/g is most likely due to the high content of metal oxide inside the pores. Intrapore formation of the metal oxide nanoparticles within the mesopores reduces the mean pore diameter also. The particles most like occupy channel intersections with larger diameter than the channel system connecting the intersections. The reduced pore volume and pore diameter was almost same for material prepared via aqueous and organometallic route. It was already discussed in our previous report [23] that in Cu/ZnO-MCM-48, instead of forming nanoparticles, ZnO coated only the inner surface when aqueous route was employed for the post-synthetic impregnation process. So it is not easy to say whether the metal oxides have coated the inner surface or have formed nanoparticles considering only N_2 -physorption results. In order to confirm the exact state of the metal oxides, techniques such as EXAFS experiments were performed to have a better insight of local environment of the metal center. The fourier-transformed (k^2 -weighted, absolute values) EXAFS spectra of ZnO impregnated MCM-48 compared with reference bulk ZnO is given in **Fig. 4** and **Fig. 5**.

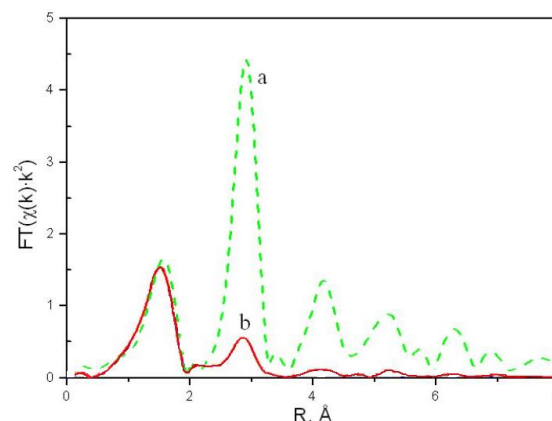


Fig. 4. EXAFS spectra of Zn modified MCM-48 Fourier-Transformed ZnK spectra: (a) ZnO as a reference and (b) ZnO-MCM-48 prepared by organometallic route.

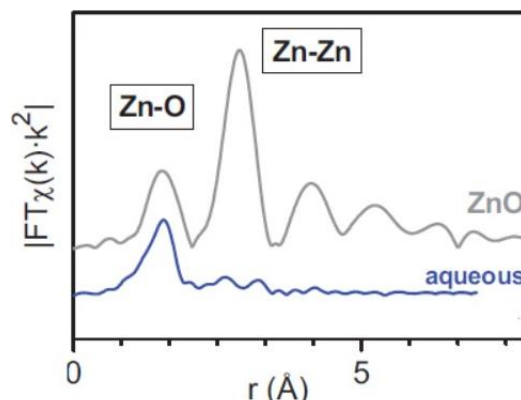


Fig. 5. EXAFS spectra of Zn modified MCM-48 Fourier-Transformed ZnK spectra: ZnO as a reference and ZnO-MCM-48 prepared by aqueous route.

The EXAFS spectra of ZnO-MCM-48 prepared by organometallic route (spectra b in Fig. 4) exhibit significant differences compared with the Zn sample prepared by aqueous route (spectra a in Fig. 5). There are also drastic differences between the Zn coordination spheres in ZnO and Zn modified MCM-48 prepared by aqueous route. The spectrum of ZnO shows different scattering features due to neighbouring shells; there is no order beyond the first neighbour of aqueous zinc in porous MCM-48 host. In particular, in the region of intense second shell in ZnO (Zn) there are only two weak scattering events are observed. Closer inspection shows that it occurs even at different distances than in ZnO. However, a complete different picture was observed when Zn is introduced by organometallic route in siliceous MCM-48 matrix.

The scattering events beyond the first neighbour were the same in ZnO and in the Zn species in MCM-48. In particular, in the region of the intense second shell in ZnO (Zn), there is a clear scattering event for the sample prepared by organometallic route. In this material the second shell coincides with the Zn shell in ZnO, but with small amplitude, indicating the formation of either extremely small or disordered ZnO particles. If the MCM-48, which was used for impregnation is not properly dried then there is a chance of interaction of diethyl zinc with absorbed water to form ZnO aggregates. Nevertheless, there is a possibility of the presence of the ZnO particles outside the porous matrix. In order to check for external bulk oxide, TEM experiment was carried out on these samples. Fig. 6 shows the TEM image of the Zn loaded sample along with EDS analysis. After impregnation and careful calcination of the sample, regular contrast variation in the TEM image shows the intactness of MCM-48 silicate framework. It is concluded that impregnation procedure and consecutive thermal treatment does not damage the host structure. No ZnO particle was observed in the TEM images attached to the external surface of the mesoporous silica support, indicating the absence of any large ZnO particle. In the EDS analysis there is a clear Zn signal at 8.7 keV. The sample was mounted on a Cu grid and for that reason there is a Cu signal in the EDS spectra. Careful investigation shows that the ZnO nano particles formed within the pore may have a maximum diameter of 2 to 2.5 nm as revealed from the TEM image. It is reliable because according to porosity result the pore diameter of pure MCM-48 has been found to be 2.5 nm. On the basis of particle size of 2 to ~2.5 nm, crystallographic data of MCM-48 (Table 2), and the density of calcined MCM-48 of $\sim 0.97 \text{ g/cm}^3$, the distribution of nano particles inside the pore has been calculated [24].

Assuming that the deposition occurs favorably at the channel intersection for the ZnO loaded sample with 17 wt % of Zn, approximately 40-50 % occupancy of channel intersection has been found. That means still there is enough free space for three-dimensional diffusion. Since the void space at the intersection is at least 3 nm in diameter as Terasaki [29] has shown experimentally from electron diffraction structure analysis for MCM-48, allowing three-dimensional diffusion without pore blockage. With the combination of EXAFS spectra and TEM image it is clear that there is a formation of ZnO

particles, which is situated inside the porous matrix. In the TEM image it is very much clear that the particles are well aligned with respect to the electron beam showing the periodicity of the silica framework. The lattice fringes show the high crystallinity of the mesoporous matrix and the dark spherical contrast inside the pore system indicates the ZnO nanoparticles of the size of the pore diameter.

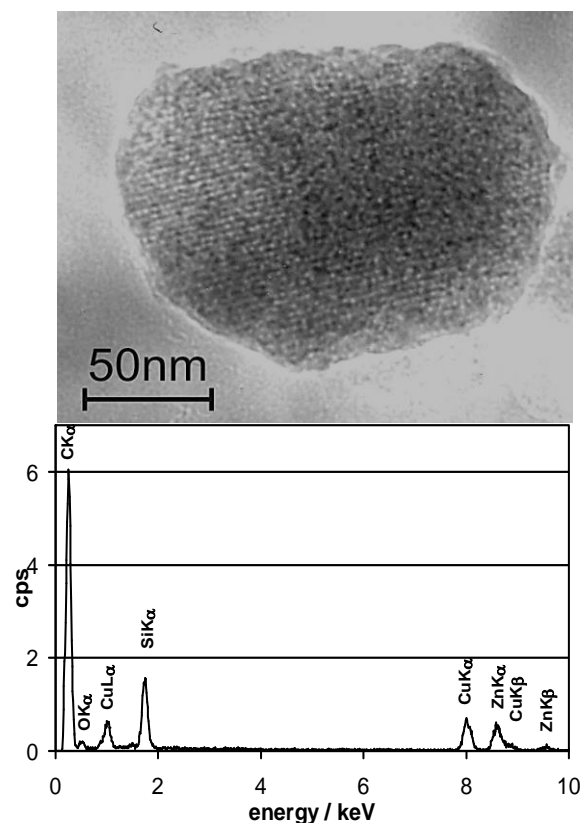


Fig. 6. TEM image of an isolated MCM-48 particle loaded with ZnO (Organometallic route) along with EDS analysis.

Table 2. Characteristic crystallographic properties of MCM-48.

Parameter	Value
Lattice parameter (as made)	94.1 Å
Lattice parameter (calcined)	83.9 Å
Cell volume (as made)	832,880 Å ³
Cell volume (calcined)	590,168 Å ³
Space group Symmetry	Ia3d
No. of channel intersection	16

Conclusion

Post-synthetic organometallic route was employed for the incorporation of metal oxide. Impregnation of the calcined MCM-48 with diethylzinc and subsequent calcination leads to incorporation of metal oxides inside the mesopore system of MCM-48 as nanoparticles reflecting the size of host mesopore. The structural properties of the resulting materials were investigated thoroughly by a combination of different physico-chemical techniques like powder XRD, N₂ Adsorption, TEM and EXAFS studies. The host structure of the mesoporous support remains intact even after calcination at temperature above 500 °C. Using

EXAFS at the zinc edge as probe for the local structure of the nanoparticle, it has been shown that zinc oxide was formed with zinc in tetrahedral coordination and a particle size of about 2-2.5 nm. The structure is disordered and reflects wurzite/spalerite staking. Pore volume as well as pore diameter decrease after Zn intake. Organometallic route is found to be effective for the formation of ZnO nanoparticles and is different from the impregnation through aqueous route which leads to surface coverage of the silicate channel wall most likely reacting with the silicate species. The composite exhibit high thermal stability as it was stable and the parent mesoporous structure was intact after metal oxide incorporation and subsequent calcination at 540 °C. This study also substantiates that only the combination of various bulk and surface analytical techniques provide a most complete picture of the nature of the composite material. Fabrication of nano-sized ZnO material stabilised in mesoporous MCM-48 support might be a promising approach towards the preparation of effective catalyst for methanol synthesis.

Acknowledgements

This work was supported by Deutsche Forschungsgemeinschaft in the frame of "Metal support interactions in heterogeneous catalysis".

Author contributions

Conceived the plan: MB, HG; Performed the experiments: MB; Data analysis: MB, HG, WG, MVB, AB; Wrote the paper: MB, HG, WG. Authors have no competing financial interests.

Reference

- Zhang, Q.; Xie, C.; Zhang, S.; Wang, A. B. Zhu.; Wang, L.; Yang, Z.; *Sens. Actuators B*. **2005**, *110*, 370.
DOI: [10.1016/j.snb.2005.02.017](https://doi.org/10.1016/j.snb.2005.02.017)
- Huang, W.J.; Fang, G.C.; Wang, L.C.; *Colloid. Surfaces. A. Physicochem. Eng. Aspects*. **2005**, *260*, 45.
DOI: [10.1016/j.colsurfa.2005.01.031](https://doi.org/10.1016/j.colsurfa.2005.01.031)
- Amapoorani, R.; Dhangayan, M.R.; Renganathan, R.J.; *Photochem. Photo Biol. A. Chem.* **1997**, *111*, 215.
DOI: [10.1016/S1010-6030\(97\)00170-6](https://doi.org/10.1016/S1010-6030(97)00170-6)
- Papavlassopoulos, H.; Mishra, Y. K.; Kaps, S; Paulowicz, I.; Abdelaziz, R.; Elbahri, M.; Maser, E.; Adlung, R.; Röhl, C.; *PLoS ONE*. **2014**, *9*, e84983.
DOI: [10.1371/journal.pone.0084983](https://doi.org/10.1371/journal.pone.0084983)
- Matsubara, K.; Fons, P.; Iwata, K.; Yamada, A.; Sakurai, K.; Tampo, N.; Niki, S.; *Thin Solid Films*. **2003**, *431*, 369.
DOI: [10.1016/S0040-6090\(03\)00243-8](https://doi.org/10.1016/S0040-6090(03)00243-8)
- Rossetti, R.; Hall, R.; Gibson, J.M.; Brus, L.E.; *J. Chem. Phys.* **1985**, *83*, 1406.
DOI: [10.1063/1.449407](https://doi.org/10.1063/1.449407)
- Ekimov, A.I.; Efros, Al. L.; Onushchenko, A.A.; *Solid State Commun.* **1985**, *56*, 921.
DOI: [10.1016/S0038-1098\(85\)80025-9](https://doi.org/10.1016/S0038-1098(85)80025-9)
- Abdullah, M.; Morimoto, T.; Okuyama, K.; *Adv. Funct. Mater.* **2003**, *13*, 800.
DOI: [10.1002/adfm.200304330](https://doi.org/10.1002/adfm.200304330)
- Mishra, Y. K.; Kaps, S.; Schuchardt, A.; Paulowicz, I.; Jin X.; Gedamu, D.; Freitag S.; Claus, M.; Wille, S.; Kovalev, A.; Gorb, S. N.; Adlung, R.; *Part. Part. Syst. Charact.* **2013**, *30*, 775.
DOI: [10.1002/ppsc.201300197](https://doi.org/10.1002/ppsc.201300197)
- Antoine, T.; Mishra, Y. K.; Trigilio, J.; Tiwari, V.; Adlung R.; Shukla, D.; *Antiviral Res.* **2012**, *96*, 363.
DOI: [10.1016/j.antiviral.2012.09.020](https://doi.org/10.1016/j.antiviral.2012.09.020)
- Zeng, H.; Duan, G.; Li, Y.; Yang, S.; Xu, X.; Cai, W.; *Adv. Funct. Mater.* **2010**, *20*, 561.
DOI: [10.1002/adfm.200901884](https://doi.org/10.1002/adfm.200901884)
- Tian, Z. R.; Voigt, J. A.; Liu J; Mckenzie, B.; Mcdermott, M. J.; Rodriguez, M. A.; Konishi, H.; Xu, H.; *Nature Materials* **2003**, *2*, 821.
DOI: [10.1038/nmat1014](https://doi.org/10.1038/nmat1014)
- Barton, T.J.; Bull, L.M.; Klemperer, W.G.; Loy, D.A.; McEnaney, B.; Misono, M.; Monson, P.A.; Pez, G.; Scherer, G.W.; Vartuli, J.C.; Yaghi, O.M. *Chem. Mater.* **1999**, *11*, 2633.
DOI: [10.1021/cm9805929](https://doi.org/10.1021/cm9805929)
- Moller, K.; Bein, T.; *Chem. Mater.* **1998**, *10*, 2950.
DOI: [10.1021/cm980243e](https://doi.org/10.1021/cm980243e)
- Wu, C.G.; Bein, T.; *Science*. **1994**, *264*, 1757.
DOI: [10.1126/science.264.5166.1757](https://doi.org/10.1126/science.264.5166.1757)
- Kinski, I.; Gies, H.; *Zeolites*. **1997**, *19*, 375.
DOI: [10.1016/S0144-2449\(97\)00085-7](https://doi.org/10.1016/S0144-2449(97)00085-7)
- Hoppe, R.; Ortlam, A.; Rathousky, J.; Schulz-Ekloff, G.; Zupal, A.; *Microporous Mater.* **1997**, *8*, 267.
DOI: [10.1016/S0927-6513\(96\)00085-5](https://doi.org/10.1016/S0927-6513(96)00085-5)
- Schulz-Ekloff, G.; Wöhrle, D.; Van Duffel, B.; Schoonheydt, R.A.; *Micropor. Mesopor. Mater.* **2002**, *51*, 91.
DOI: [10.1016/S1387-1811\(01\)00455-3](https://doi.org/10.1016/S1387-1811(01)00455-3)
- Schüth, F.; Wingen, A.; Sauer, J.; *Micropor. Mesopor. Mater.* **2001**, *465*, 44.
DOI: [10.1016/S1387-1811\(01\)00222-0](https://doi.org/10.1016/S1387-1811(01)00222-0)
- Fröba, M.; Köhn, R.; Bouffaud, G.; Richard, O.; van Tendeloo, G.; *Chem. Mater.* **1999**, *11*, 2858.
DOI: [10.1021/cm991048j](https://doi.org/10.1021/cm991048j)
- Köhn, R.; Fröba, M.; *Catal. Today*. **2001**, *68*, 227.
DOI: [10.1016/S0920-5861\(01\)00282-6](https://doi.org/10.1016/S0920-5861(01)00282-6)
- Hartmann, M.; Racouchot, S.; Bishof, C.; *Micropor. Mesopor. Mater.* **1999**, *27*, 309.
DOI: [10.1016/S1387-1811\(98\)00264-9](https://doi.org/10.1016/S1387-1811(98)00264-9)
- Gies, H.; Graboski, S.; Bandyopadhyay, M.; Grünert, W.; Tkachenko, O.P.; Klementiev, K.V.; Birkner, A.; *Micropor. Mesopor. Mater.* **2003**, *60*, 31.
DOI: [10.1016/S1387-1811\(03\)00313-5](https://doi.org/10.1016/S1387-1811(03)00313-5)
- Bandyopadhyay, M.; Birkner, A.; van den Berg, M.W.E.; Klementiev, K. V.; Schmidt, W.; Grünert, W.; Gies, H.; *Chem. Mater.* **2005**, *17*, 3820.
DOI: [10.1021/cm0484854](https://doi.org/10.1021/cm0484854)
- Bandyopadhyay, M.; Korsak, O.; van den Berg, M.W.E.; Grünert, W.; Birkner, A.; Li, W.; Schüth, F.; Gies, H.; *Micropor. Mesopor. Mater.* **2006**, *89*, 158.
DOI: [10.1016/j.micromeso.2005.09.029](https://doi.org/10.1016/j.micromeso.2005.09.029)
- Klementiev, K.V.; VIPER for Windows (Visual Processing in EXAFS Researches), freeware, www.desy.de/~klmn/viper.html.
- Ankudinov, A.L.; Ravel, B.; Rehr, J. J.; Conradson, S.D.; *Phys. Rev. B*. **1998**, *58*, 7565.
DOI: [10.1103/PhysRevB.58.7565](https://doi.org/10.1103/PhysRevB.58.7565)
- Marler, B.; Oberhagemann, U.; Vortmann, S.; Gies, H.; *Microporous Mater.* **1996**, *6*, 375.
DOI: [10.1016/0927-6513\(96\)00016-8](https://doi.org/10.1016/0927-6513(96)00016-8)
- Kaneda, M.; Tsubakiyama, T.; Carlsson, A.; Sakamoto, Y.; Ahsuna, T.; Terasaki, O.; Joo, S.H.; Ryoo, R.; *J. Phys. Chem. B*. **2002**, *106*, 1256.
DOI: [10.1021/jp0131875](https://doi.org/10.1021/jp0131875)

Advanced Materials Letters

Copyright © VBRI Press AB, Sweden
www.vbripress.com

Publish your article in this journal

Advanced Materials Letters is an official international journal of International Association of Advanced Materials (IAAM, www.iaamonline.org) published by VBRI Press AB, Sweden monthly. The journal is intended to provide top-quality peer-review articles in the fascinating field of materials science and technology particularly in the area of structure, synthesis and processing, characterisation, advanced-state properties, and application of materials. All published articles are indexed in various databases and are available download for free. The manuscript management system is completely electronic and has fast and fair peer-review process. The journal includes review article, research article, notes, letter to editor and short communications.

